Published in final edited form as:
Oncogene. 2014 January 30; 33(5): 539–549. doi:10.1038/onc.2012.632.

Aurora Kinase A Mediates Epithelial Ovarian Cancer Cell Migration and Adhesion

Thuy-Vy Do[a,b], **Fang Xiao**[a,c], **Laura E. Bickel**[a], **Andres J. Klein-Szanto**[d], **Harsh B. Pathak**[a,b], **Xiang Hua**[e], **Caitlin Howe**[a], **Shane O'Brien**[c], **Marisa Maglaty**[c], **Jeffrey A. Ecsedy**[f], **Samuel Litwin**[g], **Erica A. Golemis**[c], **Russell J. Schilder**[a,h,i], **Andrew K. Godwin**[a,b], and **Denise C. Connolly**[a,c]

[a]Women's Cancer Program, Fox Chase Cancer Center, Philadelphia, PA

[b]Department of Pathology and Laboratory Medicine, University of Kansas Medical Center, Kansas City, KS

[c]Developmental Therapeutics Program, Fox Chase Cancer Center, Philadelphia, PA

[d]Department of Pathology, Fox Chase Cancer Center, Philadelphia, PA

[e]Transgenic Facility, Fox Chase Cancer Center, Philadelphia, PA

[f]Department of Translational Medicine, Millennium Pharmaceuticals Inc., Cambridge, MA

[g]Biostatistics Facility, Fox Chase Cancer Center, Philadelphia, PA

[h]Department of Medical Oncology, Fox Chase Cancer Center, Philadelphia, PA

[i]Department of Gynecologic Medical Oncology, Thomas Jefferson University, Philadelphia, PA

Abstract

Aurora kinase A (AURKA) localizes to centrosomes and mitotic spindles where it mediates mitotic progression and chromosomal stability. Overexpression of AURKA is common in cancer, resulting in acquisition of alternate non-mitotic functions. In the current study, we identified a novel role for AURKA in regulating ovarian cancer cell dissemination and evaluated the efficacy of an AURKA-selective small molecule inhibitor, alisertib (MLN8237), as a single agent and combined with paclitaxel using an orthotopic xenograft model of epithelial ovarian cancer (EOC). Ovarian carcinoma cell lines were used to evaluate the effects of AURKA inhibition and overexpression on migration and adhesion. Pharmacologic or RNAi-mediated inhibition of AURKA significantly reduced ovarian carcinoma cell migration and adhesion and the activation-associated phosphorylation of the cytoskeletal regulatory protein SRC at tyrosine 416 ($pSRC^{Y416}$). Conversely, enforced expression of *AURKA* resulted in increased migration, adhesion and activation of SRC in cultured cells. *In vivo* tumor growth and dissemination were inhibited by alisertib treatment as a single agent. Moreover, combination of alisertib with paclitaxel, an agent commonly used in treatment of EOC, resulted in more potent inhibition of tumor growth and dissemination compared to either drug alone. Taken together, these findings support a role for AURKA in EOC dissemination by regulating migration and adhesion. They also point to the

Corresponding author address: Dr. Denise C. Connolly, Developmental Therapeutics Program, 333 Cottman Ave., W310, Philadelphia, PA 19111, Phone: 215-728-1004; FAX: 215-728-2741, Denise.Connolly@fccc.edu.

Conflicts of interest: none
The authors have no conflicts of interest to disclose.

Supplementary Information
Supplementary Information accompanies the paper.

potential utility of combining AURKA inhibitors with taxanes as a therapeutic strategy for the treatment of EOC patients.

Keywords

Aurora kinase A; SRC; ovarian cancer; migration; alisertib; adhesion

Introduction

The majority of women with epithelial ovarian cancer (EOC) are diagnosed at advanced stage when disease has spread beyond the ovary. Peritoneal dissemination and ascites are a significant cause of patient morbidity and mortality. Although most patients respond to aggressive surgical debulking and platinum and taxane-based combination chemotherapy, the majority experience disease recurrence and ultimately drug resistance, making EOC the most lethal gynecologic malignancy (1). Hence, there is a critical need to identify additional therapeutic agents that target pathways specific to EOC progression.

Aurora kinases are a family of serine/threonine kinases consisting of three members, AURKA, AURKB and AURKC, which are essential regulators of mitosis (2, 3). The expression and activity of Aurora kinases are tightly regulated, with dysregulation leading to genetic instability, aneuploidy and cell death (3). AURKA plays critical roles in mitotic entry, centrosome function and bipolar spindle assembly. AURKA is implicated in the regulation of the G2/M transition; inhibition of AURKA expression results in G2/M arrest and apoptosis, while ectopic expression allows cells to bypass the G2/M DNA damage checkpoint (2). Overexpression of AURKA is a common feature of EOC and other solid tumors (3, 4) and can be related to gene amplification, transcriptional activation or delayed protein degradation (5–11). High levels of AURKA in primary ovarian tumors is associated with supernumerary centrosomes and overall decreased survival (12), suggesting that AURKA plays an important role in ovarian cancer biology.

In addition to well-established roles of AURKA in cancer-associated genetic instability and aneuploidy, recent studies implicate a potential role for AURKA in metastasis (13–17). High levels of AURKA expression in clinical head and neck squamous cell carcinoma (HNSCC) specimens is associated with invasion, advanced stage and poor prognosis (14, 18). The mechanisms by which AURKA influences cell migration and invasion are not completely defined, although studies suggest roles for RAS (19), AKT (13, 20), MAPK (18) and RALA (21).

Prior work suggests the possibility that AURKA may exert its effects on motility through a group of closely interacting proteins that regulate focal adhesion turnover and motility, including NEDD9, SRC and FAK (22). NEDD9 is a scaffolding protein that has dual functions at focal adhesions and at centrosomes during interphase and mitosis, respectively (23, 24). It is critical for activation of SRC and FAK, and in regulating factors involved in the cytoskeletal reorganization and focal adhesion turnover required for migration and cell rounding during mitosis. Recent work showed NEDD9 is also an *in vivo* mediator of metastasis in mouse models of melanoma and lung cancer (25, 26). Notably, association with NEDD9 is required for AURKA activation, and overexpression of NEDD9 results in supernumerary centrosomes and multipolar spindles, similar to effects observed with AURKA overexpression (27).

AURKA has become a target of interest for therapeutic intervention because of its frequent activation in human tumors. There are a number of available Aurora kinase inhibitors that

have dual-specificity for AURKA and AURKB, including MK-0457 and PHA-739358. *In vivo* treatment with these agents results in phenotypes consistent with abrogation of AURKB function (3, 28). More recently, AURKA-selective inhibitors have been developed. Among these, MLN8054, an ATP-competitive, reversible inhibitor is >150-fold more selective for AURKA than AURKB (29). In preclinical studies, MLN8054 inhibited human colon and prostate xenograft growth, an effect that was sustained after drug withdrawal (29). Consistent with inhibition of AURKA activity, analysis of primary tumors showed accumulation of cells in mitotic arrest and undergoing apoptosis (29). A second-generation compound, alisertib (MLN8237), exhibits even greater specificity for AURKA, with >200-fold greater selectivity for AURKA than AURKB (30).

The current study tests the hypothesis that AURKA plays a role in EOC growth and dissemination. The effects of AURKA loss- and gain-of-function were assessed in cultured EOC cells and the effects of alisertib on the growth and dissemination of orthotopic ovarian xenografts. We report that either pharmacologic or RNAi-mediated inhibition of AURKA resulted in decreased migration and adhesion of EOC cells. In addition, inhibition of AURKA expression or activity resulted in significantly reduced SRC activation, as measured by phosphorylation at tyrosine 416 ($pSRC^{Y416}$). Conversely, enforced expression of *AURKA* resulted in increased migration, adhesion and $pSRC^{Y416}$ levels. Alisertib treatment alone or combined with paclitaxel significantly reduced the growth and dissemination of orthotopic EOC xenografts. Collectively, these observations support the hypothesis that AURKA plays an important role in EOC dissemination *in vitro* and *in vivo* and further suggest the potential clinical utility of AURKA inhibition alone or in conjunction with taxanes for the treatment of EOC.

Results

AURKA regulates migration in ovarian carcinoma cells

A panel of ten cell lines was screened for highly active AURKA using a $pAURKA^{T288}$ ELISA (Supplementary Fig. S1A). The specificity of the assay was confirmed in control experiments showing a sharp induction of $pAURKA^{T288}$ levels in cells treated with nocodazole or transiently transfected with an *AURKA* expression construct (Supplementary Fig. S1B–C). Two cell lines with high levels of activated AURKA (OVCAR-5 and SKOV3ip2) and two cell lines with low levels of activated AURKA (A2780 and OVCA433) were selected for studies evaluating the effects of AURKA inhibition or overexpression.

To determine if AURKA plays a role in EOC dissemination, *in vitro* experiments were performed to evaluate the effects of AURKA loss- or gain-of-function on migration and adhesion. First, alisertib sensitivity and dose-response were assayed by ELISA to measure $pAURKA^{T288}$ levels in cells exposed to increasing concentrations of drug (Supplemental Figure S1D). Cell lines with high endogenous levels of activated AURKA (OVCAR-5 and SKOV-3ip2) exhibited significant dose-dependent inhibition of $pAURKA^{T288}$ levels at alisertib concentrations of 10 nmol/L and higher ($p<0.0001$). A2780 and OVCA-433 cells exhibit lower endogenous levels of $pAURKA^{T288}$, and significant inhibition was observed at concentrations of 25 nmol/L alisertib and higher ($p<0.001$). To ensure that the doses of alisertib used in subsequent assays were not cytotoxic, cells were exposed to increasing concentrations of alisertib for 48–72 hr to evaluate the effects on proliferation and apoptosis (Supplementary Fig. S2A–E). Alisertib doses (10–50 nmol/L) that showed little or no significant effects on proliferation or apoptosis were used for subsequent assays. The effect of inhibition of AURKA kinase activity on migration was assessed using trans-well chemotactic migration assays. Alisertib inhibited OVCAR-5 cell migration in a concentration-dependent manner, with a 19% and 40% and 60% ($P < 0.01$) decrease in migration of cells treated with 10, 25, and 50 nmol/L, respectively (Fig. 1A). Similar results

were observed in SKOV3ip2 cells, where 10 25 and 50 nmol/L alisertib reduced migration by 28%, 47% and 59% ($P < 0.001$, Fig. 1B). Alisertib treatment also inhibited migration in cells with low endogenous AURKA activity; drug treatment (10, 25, and 50 nmol/L, respectively) inhibited cell migration by 32%, 47% and 56% in A2780 cells and by 23 %, 31% and 45% in OVCA433 cells ($P < 0.0001$, Supplemental Figure S3). These results show that alisertib treatment decreases the migratory capacity of EOC cells.

Prior studies (24, 31) showed that AURKA functions are mediated through interactions with NEDD9, a scaffolding protein that regulates SRC and FAK. Therefore, we investigated the potential role of these proteins in AURKA-mediated migration by evaluating their expression and activation in cells treated with increasing concentrations of alisertib. Activation of each of these proteins depends on distinct phosphorylation events that can be detected by a mobility shift in NEDD9 and phosphorylation of specific tyrosine residues in SRC and FAK. Increasing doses of alisertib (10, 25, 50 nmol/L) resulted in a concentration-dependent decrease in phosphorylation of SRC at tyrosine 416 ($pSRC^{Y416}$) in OVCAR-5 and SKOV3ip2 cells (Fig. 1A–B) indicating decreased SRC activity. Alisertib had negligible effects on the levels or mobility of NEDD9 or the levels of $pFAK^{Y861}$ in either cell line (Fig. 1 and not shown). A slight increase in total AURKA levels was observed in alisertib-treated cells; though the reasons for this are unclear, AURKA activity measured by ELISA clearly showed significant ($P < 0.0001$) concentration-dependent decreases in $pAURKA^{T288}$ levels in response to alisertib (Supplemental Figure S1D).

Cell-free assays with 1 μM alisertib show inhibition of many kinases including SRC (30); however, the doses of alisertib used in the current studies (10 – 50 nmol/L) are low and not predicted result in off-target effects resulting in direct interference with SRC kinase activity. To confirm the specificity of the effects of AURKA inhibition on migration and SRC activation, we evaluated RNAi-mediated silencing of *AURKA* with two individual *AURKA*-targeting siRNAs and a non-targeting scrambled control siRNA (Figure 2). Efficient knockdown of *AURKA* by both targeting siRNAs was confirmed by western blot analysis of AURKA protein levels (Fig. 2A–B). In addition, transfection with *AURKA*-targeting siRNAs, si-28 and si-29, decreased migration of OVCAR-5 cells by 35% to 42% ($P < 0.01$) and SKOV3ip2 cells by 34% ($P < 0.0001$) compared to scrambled siRNA controls (Fig. 2A–B). Consistent with alisertib treatment, knockdown of *AURKA* with either siRNA resulted in decreased $pSRC^{Y416}$, but no changes in NEDD9 mobility or $pFAK^{Y861}$ levels (Fig. 2A–B and data not shown). Collectively, these results demonstrate that inhibition of AURKA activity or expression significantly inhibits cell migration and SRC activation in EOC cell lines.

We next tested whether transient expression of *AURKA* in cells with low endogenous AURKA activity stimulated migration and SRC activation. Expression of *AURKA* increased migration by 75% ($P < 0.0001$) in A2780 and 64% ($P < 0.0001$) in OVCA433 cells (Fig. 3A–B). Separate assays confirmed that increased migration was not due to increased cell proliferation (not shown). Western blot analyses showed A2780 and OVCA433 cells overexpressing *AURKA* exhibited increased levels of $pSRC^{Y416}$ (Fig. 3A–B). Taken together, these results show that AURKA plays a critical role in EOC cell migration, and that activation of SRC strongly correlates with AURKA expression and activation, and hence may play a role in AURKA-mediated motility.

AURKA regulates adhesion in ovarian carcinoma cells

The ability of ovarian cancer cells to shed from the primary tumor and adhere at secondary sites within the abdominal cavity is central to the process of EOC dissemination (32). We showed that AURKA mediates tumor cell motility and the activity of SRC, a tyrosine kinase that regulates both cell motility and adhesion (33). Therefore, we next assessed the effects of

increasing concentrations of alisertib on tumor cell adhesion on type I collagen or BSA (negative control). Alisertib treatment resulted in a concentration-dependent decrease in adhesion to type I collagen; relative to vehicle-treated cells, adhesion was decreased by 35% and 46% ($P < 0.0001$) in OVCAR-5 cells in the presence of 25 and 50 nmol/L alisertib, and by 55%, 58% and 62% ($P < 0.0001$) in SKOV3ip2 cells in the presence of 10, 25 and 50 nmol/L alisertib, respectively (Fig. 4A–B).

Similar to pharmacologic inhibition, siRNA knockdown of *AURKA* decreased adhesion by 36–41% in OVCAR-5 and 38–44% in SKOV3ip2 cells compared to controls (Figure 4C–D, $P < 0.001$). In A2780 and OVCA433 cells, overexpression of *AURKA* increased adhesion by 3.3-fold and 2.7-fold, respectively (Fig. 4E–F, $P < 0.0001$). These results demonstrate that AURKA regulates EOC cell adhesion to type I collagen.

Alisertib sensitizes ovarian carcinoma cells to paclitaxel *in vitro*

Data showing that AURKA mediates ovarian carcinoma cell growth and dissemination *in vitro* suggest it may be a good therapeutic target for treatment of EOC. Interestingly, while overexpression of AURKA has been shown to confer resistance to the effects of taxanes in HeLa cells (34), pharmacologic inhibition or genetic depletion of AURKA sensitizes HeLa, HNSCC, pancreatic, esophageal, lung and colon carcinoma cells to taxanes (35–39). Taxanes are a component of standard front-line chemotherapy for EOC, and the development of resistance to these agents is common (40). Therefore, we used the Chou-Talalay method (41) to determine the molar ratio of alisertib and paclitaxel that results in a synergistic combination index (CI) in limiting the growth of OVCAR-5 cells *in vitro*. In these cells, the IC_{50} value for alisertib alone was 315 nmol/L, but when combined with paclitaxel at a 16:1 molar ratio (alisertib:paclitaxel) the IC_{50} decreased to 35 nmol/L (Supplementary Table S1). Similarly, the IC_{50} for paclitaxel was 4 nmol/L, but when combined with alisertib at a 40:1 ratio, the IC_{50} decreased to 1.2 nmol/L (Supplementary Table S1). These data demonstrate potent synergy between alisertib and paclitaxel *in vitro*, and suggest that combination of these agents may be effective.

Alisertib treatment decreases ovarian tumor growth and dissemination *in vivo*

An orthotopic mouse model was used to determine the therapeutic efficacy of alisertib alone or in combination with paclitaxel *in vivo*. Briefly, mice (n=80) were given unilateral injections of OVCAR-5-pWZL-Luc cells suspended in Matrigel into the intrabursal (i.b.) space surrounding the left ovary. One week post-injection, the presence of tumor cells was confirmed by bioluminescent imaging (BLI) and the mice (n=16/group) were randomly divided into five treatment groups: 1) vehicle, 2) 20 mg/kg alisertib, 3) 30 mg/kg alisertib, 4) 5 mg/kg paclitaxel and 5) 20 mg/kg alisertib + 5 mg/kg paclitaxel. Tumor growth was monitored by weekly BLI (Fig. 5A) and the log-transformed total flux data showed significantly decreased tumor growth rates in mice treated with alisertib (20 or 30 mg/kg alisertib, $P < 0.05$) compared to vehicle-treated mice (Fig. 5B). While BLI can be used as a surrogate measure of *in vivo* tumor growth, this method is subject to limitations including light absorption and scattering in tissues, limited spatial resolution (1–3 mm) and diminished signal detection in deep tissues (42); therefore, endpoint analyses of tumor size and dissemination are essential to determine differences in tumor growth in drug-treated animals. In accord with the BLI data, analyses of the primary ovarian tumor volumes showed significant tumor growth inhibition (TGI) in alisertib-treated mice compared to controls ($P < 0.001$, Fig. 5C and D). Overall, treatment with 20 mg/kg and 30 mg/kg alisertib resulted in 51% and 49% TGI, respectively. These results demonstrate that alisertib exhibits significant single agent activity toward orthotopic human EOC xenografts.

To assess the effect of drug treatment on tumor dissemination, tumor nodules were enumerated and 1) small nodules < 1mm diameter and 2) nodules ≥ 1mm diameter were further quantified for volume (Supplementary Fig. S4A–C). Once-daily treatment with 20 mg/kg or 30 mg/kg alisertib resulted in a 26% or 50% reduction in the total number of tumor nodules, respectively, (Fig.5F), and a 44% or 43% reduction in the mean volume of tumor nodules, respectively, relative to vehicle-treated mice (Supplementary Fig. S4C). Although the trend did not reach statistical significance, these data suggest that once-daily dosing of alisertib treatment reduced both the number and volume of secondary lesions.

An independent experiment was conducted to determine the effect of twice-daily (BID) dosing with 30 mg/kg alisertib. In addition to highly significant 81% TGI ($P < 0.0001$), BID dosing had a profound effect on the capacity for tumor to spread beyond the primary injection site; the number of tumor nodules was reduced by 92% ($P < 0.0001$) in alisertib-treated mice compared with controls (Fig 5F–G). Taken together, these data show that alisertib treatment significantly inhibits both ovarian tumor growth and dissemination.

Alisertib sensitizes ovarian carcinoma cells to paclitaxel *in vivo*

In vivo TGI was also evaluated in mice treated with paclitaxel alone or in combination with 20 mg/kg alisertib. The TGI observed in paclitaxel-treated mice was similar (46%) to either concentration of alisertib alone (Fig. 5D, $P < 0.001$). However, when paclitaxel was combined with alisertib, the effect was significantly greater than either drug alone, with an overall TGI of 63% (Fig. 5D, $P < 0.0001$ compared to vehicle and $P < 0.05$ compared to 30 mg/kg alisertib or 5 mg/kg paclitaxel). The total number of tumor nodules in the paclitaxel and combination therapy groups was significantly lower than vehicle-treated mice ($P < 0.05$ and $P < 0.001$, respectively), and the number of nodules in the combination therapy group was significantly less ($P < 0.01$) than in either of the alisertib monotherapy groups (Fig. 5E). The number of measurable nodules and the mean volume were significantly decreased in the paclitaxel and combination therapy groups ($P \leq 0.01$, Supplementary Fig. S4B–C). Collectively, these data show that alisertib is effective as a single agent, and the addition of paclitaxel results in further reduction of primary tumor volume and secondary lesions.

Alisertib-mediated TGI correlates with decreased AURKA activity

Tumors were subjected to IHC staining to evaluate the effects of drug treatment on levels of $pAURKA^{T288}$, $pHisH3^{S10}$ and cleaved caspase-3 (Fig. 6A and Supplementary Table S2). Consistent with the selectivity for AURKA, $pAURKA^{T288}$ levels were lower in alisertib- and combination therapy-treated mice (Fig. 6A). Levels of $pAURKA^{T288}$ in tumors were also quantified by ELISA, demonstrating a significant reduction (28%) in tumors isolated from alisertib-treated mice compared to vehicle or paclitaxel-treated mice (Fig. 6B). Further reduction in $pAURKA^{T288}$ levels (65%) were observed in mice BID dosing of alisertib (Fig. 6C).

In contrast, tumors from drug- and vehicle-treated mice exhibited similar levels of $pHisH3^{S10}$ staining (Supplementary Table S2), suggesting that AURKB activity was not altered by drug treatment. No significant differences were observed in cleaved caspase-3 staining among any of the treatment groups (data not shown). These observations are consistent with *in vitro* results showing that alisertib treatment did not dramatically affect proliferation or apoptosis (Supplementary Fig. S2). Densitometric analyses of immunoblots showed a significant reduction in $pSRC^{Y416}$ levels in tumors from mice treated with 20 mg/kg alisertib and paclitaxel (Supplementary Fig. S5A–B), but no differences in total SRC, NEDD9 or AURKA were detected among any of the treatment groups (Supplementary Fig. S5C and data not shown).

Discussion

Herein, we described a previously unappreciated role for AURKA in mediating ovarian cancer cell dissemination, with findings strongly implicating an AURKA and SRC pathway as an important signaling node in EOC progression. The mechanism of action for a number of Aurora family kinase inhibitors has been investigated using xenograft models. In mice harboring human EOC xenografts, treatment with the pan-Aurora kinase inhibitor MK-0457 resulted in TGI accompanied by decreased proliferation and increased apoptosis (43). However, the low levels of mitotic arrest and apoptosis induced by this and other Aurora kinase family inhibitors does not fully account for the TGI observed (29, 43, 44). The terminal phenotypes observed with pan-Aurora kinase inhibitors (e.g., MK-0457 and AMG 900) include decreased $pHisH3^{S10}$ levels and accumulation of polyploid cells, suggesting AURKB inhibition plays a significant role in anti-tumor effects mediated by these agents (29, 43–45).

In contrast to pan-Aurora kinase inhibitors, AURKA-specific agents exhibit distinct effects. Treatment of cultured cells or xenograft-bearing mice with AURKA-specific inhibitors (e.g., MK-5108 or MLN8054) resulted in increased levels of $pHisH3^{S10}$ reflecting an accumulation of mitotic cells in tumors due to increased AURKB activity (29, 37), demonstrating the selectivity of these agents for AURKA. In MLN8054-treated mice with colon or prostate xenografts, mitotic arrest and modest activation of caspase-3 induced by AURKA inhibition was proposed to cause the observed TGI (29). In contrast, in our study, although $pAURKA^{T288}$ levels were significantly decreased in alisertib-treated mice, the levels of cleaved caspase-3 and $pHisH3^{S10}$ were not significantly different among alisertib- and vehicle-treated mice. The reasons for these differences are unclear, but are unlikely related to pharmacokinetic/pharmacodynamic differences between alisertib and MLN8054 as the half lives of these agents *in vivo* are similar (J. Ecsedy, personal communication).

The absence of significant effects of alisertib on proliferation of tumors *in vivo* suggests the inhibitory effects of alisertib are not mediated entirely by mitotic inhibition (46) and that other mechanisms may contribute to diminshed tumor growth and dissemination. Other potential mechanisms may include induction of cellular senescence or anoikis. For example, MLN8054 has been shown to confer changes associated with cellular senescence both *in vitro* and *in vivo* (47). The significantly decreased levels of SRC activation observed in conjunction with pharmacologic or genetic inhibition of AURKA are likely to directly contribute to the observed loss of cellular attachment capacity and motility. Notably, we previously showed that combination of the SRC family inhibitor dasatinib and Aurora kinase inhibitors results in cellular attachment defects that contribute to the specific elimination of cells undergoing dysregulated mitosis and polyploidy (48). The loss of cellular motilty and adhesion may also prevent ovarian carcinoma cells from attaching at secondary sites in the peritoneal cavity, a process critical to ovarian cancer dissemination (49).

Consistent with observations in other cancer models (35–39), our data show that inhibition of AURKA sensitized EOC cells to the effects of paclitaxel *in vitro* and *in vivo*. These results support the use of alisertib and paclitaxel for patients, and this combination therapy is currently under evaluation in a Phase I/II clinical trial (http://clinicaltrials.gov). The finding that AURKA inhibition in cultured cells and alisertib and paclitaxel treatment of EOC xenografts results in decreased SRC activation suggests another potentially interesting signaling node for dual therapeutic targeting. Previous work (48) demonstrated the capacity for AURKA and SRC interaction and cross phosphorylation *in vitro*, and the combination of Aurora kinase inhibitors with dasatinib potentiated EOC cell death. Hence, further studies evaluating the combined inhibition of AURKA and SRC may be of clinical interest.

Materials and Methods

Cell culture and transfection

Human EOC cell lines and medium used: OVCAR-5 and A2780 in RPMI with 10% FBS and 0.25 units/mL insulin (Novo Nordisk, Princeton, NJ); SKOV3-luc-D3 (Caliper Life Sciences, Hopkinton, MA) and SKOV3ip2-luc-D3 cells, hereafter referred to as SKOV3ip2, in McCoy's 5A with 10% FBS, 0.25 units/mL insulin and 500 μg/mL G418; OVCA433 in MEM with 10% FBS, non-essential amino acids and sodium pyruvate. SKOV3ip2 was established by isolating tumor cells from ascites that developed in a severe combined immunodeficient (SCID) mouse after injection with SKOV3-luc-D3 cells (TVD and DCC, unpublished data). Plasmids (pcDNA3.1-AURKA-RFP and pcDNA3.1-RFP) were transiently transfected using LT1 (Mirus Bio, LLC, Madison, WI) or Lipofectamine 2000 (Life Technologies, Grand Island, NY). *AURKA* knockdown was achieved by transfecting cells twice (24 h apart) with 50 nmol/L *AURKA*, or scrambled non-targeting siRNAs (Thermo Scientific, Rockford, IL) using Lipofectamine 2000. The AURKA targeting siRNAs used were the siRNA oligos (J-003545, Thermo Scientific) with the following sequences: (si#28) - 5′-UUCUUAGACUGUAUGGUUA-3′, and si#29) - 5′-AAUAGGAACACGUGCUCUA-3′. OVCAR-5 cells were transduced with a retroviral firefly luciferase construct (pWZL-Luc, a gift from Dr. Maureen Murphy) using standard methods (50). Stably transduced cells were selected in the presence of 75 μg/mL Hygromycin B (Life Technologies).

Immunoblot analysis

Cells were lysed in Mammalian Protein Extraction Reagent (MPER™) supplemented with Halt™ Phosphatase Inhibitor Cocktail (Thermo Scientific) and Complete™ Mini Protease Inhibitor Cocktail (Roche Diagnostics, Indianapolis, IN), and protein concentrations determined using the BCA assay (Thermo Scientific). Proteins were resolved on 4–12% gradient SDS-PAGE gels (Life Technologies) and transferred to PVDF membrane. Membranes were blocked in nonfat dry milk, incubated overnight at 4°C in primary antibody, followed by HRP-conjugated secondary antibody (GE Healthcare, Pittsburgh, PA) and signal detected with SuperSignal West Pico Chemiluminescent Substrate (Thermo Scientific). Anti-phospho: SRC-tyrosine^{416} (pSRC^{Y416}), AURKA-threonine^{288} (pAURKA^{T288}), histone H3-serine^{10} (pHisH3^{S10}) and anti-β-Actin were from Cell Signaling (Boston, MA); anti-SRC from Millipore (Billerica, MA), and anti-phospho-FAK-tyrosine^{861} (pFAK^{Y861}) from Life Technologies. Anti-NEDD9 clone 2G9 was previously described (27).

Migration and Adhesion assays

Migration was assayed and quantified as described (51). Briefly, 2.5 - 5 × 10^4 cells were suspended in media with 2.5% FBS and seeded in triplicate in 24-well plates containing inserts (8.0 μm pores) coated on the underside with type I collagen (10 μg/mL). Complete media was placed in the bottom chamber, and plates were incubated for 20 h at 37°C in 5% CO_2. Cells were fixed with 4% paraformaldehyde and stained with crystal violet. Bright-field images (10× magnification) of five fields/insert were acquired with a CCD camera coupled to a Nikon Eclipse E800 microscope (Melville, NY) using Nikon Act-1C software; migrated cells were counted, and the mean number of cells/field ± SEM calculated. Adhesion was assayed by plating cells in OPTI-MEM (Life Technologies) in quadruplicate on 96-well plates pre-coated with BSA (control) or 10 μg/mL type I collagen. Cells pre-treated for 6 h with drug or vehicle were allowed to adhere for 30 min to 1 h. Wells were washed, fixed with 4% paraformaldehyde and stained with crystal violet. Adhered cells were counted in five fields (at 10× magnification), and the mean number of cells/field ± SEM calculated. Statistical analysis was performed with Prism 5.0 (GraphPad Software, La Jolla,

CA) using either the Wilcoxon matched-pairs signed rank or repeated measures ANOVA, followed by Tukey's multiple comparison tests; $P < 0.05$ was considered significant.

Orthotopic xenografts and *in vivo* bioluminescent imaging

All procedures involving mice were approved by the Fox Chase Cancer Center (FCCC) Institutional Animal Care and Use Committee (IACUC). Seven to fourteen week-old female C.B-17 SCID mice (FCCC Laboratory Animal Facility and Taconic, Cranbury, NJ) were used for intrabursal (i.b.) injections as described (52). Mice were given unilateral i.b. (left side) injections of OVCAR-5-pWZL-Luc cells (2×10^5) suspended in 5 μg/μl final concentration of BD Matrigel™ Matrix High Concentration (BD Biosciences, San Jose, CA). Baseline BLI scans were acquired using the IVIS Spectrum (Caliper Life Sciences, Hopkinton, MA) as described (52) to confirm the presence of tumors. Alisertib (Millennium Pharmaceuticals, Inc., Cambridge, MA) was suspended in 10% 2-hydroxypropyl-β-cyclodextrin (Sigma-Aldrich, St. Louis, MO) with 1% sodium bicarbonate and 20 or 30 mg/kg administered orally once daily (QD) or twice daily (BID), using a 5 days on/2 days off schedule. Paclitaxel (FCCC Pharmacy) was diluted in PBS and 5 mg/kg was administered once weekly by intraperitoneal (i.p.) injection. Mice were treated for two weeks and tumor growth monitored by weekly BLI.

Regions of interest (ROIs) of identical size encompassing the luminescent signal were assigned, and the sum of the total flux from dorsal and ventral images was calculated for each mouse using Living Image software (Caliper Life Sciences). The mean total flux ± SEM for each treatment group was subjected to log transformation to calculate the mean growth rate for each treatment group. Statistical analyses were performed by subjecting pairs of data sets to the Wilcoxon two-sample test; $P < 0.05$ was considered significant.

Tissue preparation and immunohistochemistry

Mice were euthanized by CO_2 inhalation, necropsied and examined for gross abnormalities. Reproductive tracts were removed and photographed and caliper measurements of tumor length (l) and width (w) were made and tumor volume ($l \times w^2 \times 0.5$) calculated. The total number of tumor nodules were counted and classified as: 1) small nodules <1 mm diameter and 2) 'measurable nodules' ≥1 mm diameter. The volume of small nodules was estimated using the formula for a sphere, $(4/3) \times \pi r^3$, where the radius (r) was estimated at 0.5 mm, and measurable nodule volume calculated as described for tumors. The volume of tumor nodules for each animal was calculated by adding the volumes of the small and 'measurable' nodules. Portions of tumors were either snap frozen in liquid nitrogen or fixed in 10% (v/v) neutral buffered formalin and paraffin embedded. Tissue sections were stained with hematoxylin and eosin and reviewed by a pathologist (A.K.-S.). Tumor tissue microarrays were made with duplicate cores of primary tumors (n=12/group) and used for immunohistochemical (IHC) staining with pAURKA^{T288} antibody (Bethyl Laboratories, Montgomery, TX) as described (53). Images were acquired with a Nikon Eclipse E800 microscope and CCD camera with the same exposure settings.

Phosphorylated AURKA ELISA assay

Levels of pAURKA^{T288} present in protein lysates of tumors were assayed using an enhanced chemiluminescent ELISA (MesoScale Discovery™, Gaithersburg, MD) according to manufacturers' instructions.

Supplementary Material

Refer to Web version on PubMed Central for supplementary material.

Acknowledgments

The authors gratefully acknowledge Drs. Maureen Murphy and Timothy Yen for helpful discussions and critical review of this manuscript. We also thank Dr. Maureen Murphy for providing access to the Guava EasyCyte system, and Dr. Greg Enders for providing access to the Nikon Eclipse microscope. This work was supported by R01 CA136596, Tobacco Settlement funding from the State of Pennsylvania and Fox Chase Cancer Center via institutional support of the Keystone Program in Personalized Risk and Prevention (to DCC); Ovarian Cancer Research Fund Program of Excellence Award (to TVD); Ovarian SPORE P50 CA083638 (Project 4 to DCC, AKG and EAG and Pilot Award to TVD); R01 CA63366 (to EAG); R01 CA140323 (to AKG); and the Fox Chase Cancer Center Core Grant NCI P30 CA006927. The following Fox Chase Cancer Facilities were used: Laboratory Animal, Transgenic, Cell Culture, Biological Imaging, Histopathology, Biosample Repository and Biostatistics and Bioinformatics.

References

1. Jemal A, Siegel R, Ward E, Hao Y, Xu J, Murray T, et al. Cancer statistics, 2008. CA Cancer J Clin. 2008 Mar-Apr;58(2):71–96. [PubMed: 18287387]
2. Gautschi O, Heighway J, Mack PC, Purnell PR, Lara PN, Gandara DR. Aurora kinases as anticancer drug targets. Clin Cancer Res. 2008; 14(6):1639–1648. 2008. [PubMed: 18347165]
3. Keen N, Taylor S. Aurora-kinase inhibitors as anticancer agents. Nat Rev Cancer. 2004 Dec; 4(12): 927–936. [PubMed: 15573114]
4. Marumoto T, Honda S, Hara T, Nitta M, Hirota T, Kohmura E, et al. Aurora-A kinase maintains the fidelity of early and late mitotic events in HeLa cells. J Biol Chem. 2003 Dec 19; 278(51):51786–51795. [PubMed: 14523000]
5. Gritsko TM, Coppola D, Paciga JE, Yang L, Sun M, Shelley SA, et al. Activation and overexpression of centrosome kinase BTAK/Aurora-A in human ovarian cancer. Clin Cancer Res. 2003 Apr; 9(4):1420–1426. [PubMed: 12684414]
6. Hsu LC, Kapali M, DeLoia JA, Gallion HH. Centrosome abnormalities in ovarian cancer. Int J Cancer. 2005 Feb 20; 113(5):746–751. [PubMed: 15499629]
7. Lassmann S, Shen Y, Jutting U, Wiehle P, Walch A, Gitsch G, et al. Predictive value of Aurora-A/STK15 expression for late stage epithelial ovarian cancer patients treated by adjuvant chemotherapy. Clin Cancer Res. 2007 Jul 15; 13(14):4083–4091. [PubMed: 17634533]
8. Tanner MM, Grenman S, Koul A, Johannsson O, Meltzer P, Pejovic T, et al. Frequent amplification of chromosomal region 20q12-q13 in ovarian cancer. Clin Cancer Res. 2000 May; 6(5):1833–1839. [PubMed: 10815905]
9. Chung CM, Man C, Jin Y, Jin C, Guan XY, Wang Q, et al. Amplification and overexpression of aurora kinase A (AURKA) in immortalized human ovarian epithelial (HOSE) cells. Mol Carcinog. 2005 Jul; 43(3):165–174. [PubMed: 15880741]
10. Hu W, Kavanagh JJ, Deaver M, Johnston DA, Freedman RS, Verschraegen CF, et al. Frequent overexpression of STK15/Aurora-A/BTAK and chromosomal instability in tumorigenic cell cultures derived from human ovarian cancer. Oncol Res. 2005; 15(1):49–57. [PubMed: 15839305]
11. Lassus H, Staff S, Leminen A, Isola J, Butzow R. Aurora-A overexpression and aneuploidy predict poor outcome in serous ovarian carcinoma. Gynecol Oncol. 2011 Jan; 120(1):11–17. [PubMed: 20937525]
12. Landen CN Jr, Lin YG, Immaneni A, Deavers MT, Merritt WM, Spannuth WA, et al. Overexpression of the centrosomal protein Aurora-A kinase is associated with poor prognosis in epithelial ovarian cancer patients. Clin Cancer Res. 2007 Jul 15; 13(14):4098–4104. [PubMed: 17634535]
13. Guan Z, Wang XR, Zhu XF, Huang XF, Xu J, Wang LH, et al. Aurora-A, a negative prognostic marker, increases migration and decreases radiosensitivity in cancer cells. Cancer Res. 2007 Nov 1; 67(21):10436–10444. [PubMed: 17974987]
14. Reiter R, Gais P, Jutting U, Steuer-Vogt MK, Pickhard A, Bink K, et al. Aurora kinase A messenger RNA overexpression is correlated with tumor progression and shortened survival in head and neck squamous cell carcinoma. Clin Cancer Res. 2006 Sep 1; 12(17):5136–5141. [PubMed: 16951231]

15. Tong T, Zhong Y, Kong J, Dong L, Song Y, Fu M, et al. Overexpression of Aurora-A contributes to malignant development of human esophageal squamous cell carcinoma. Clin Cancer Res. 2004 Nov 1; 10(21):7304–7310. [PubMed: 15534106]
16. Wan XB, Long ZJ, Yan M, Xu J, Xia LP, Liu L, et al. Inhibition of Aurora-A suppresses epithelial-mesenchymal transition and invasion by down-regulating MAPK in nasopharyngeal carcinoma cells. Carcinogenesis. 2008 Oct; 29(10):1930–1937. [PubMed: 18667445]
17. Zhang H, Chen X, Jin Y, Liu B, Zhou L. Overexpression of Aurora-A promotes laryngeal cancer progression by enhancing invasive ability and chromosomal instability. Eur Arch Otorhinolaryngol. 2012 Feb; 269(2):607–614. [PubMed: 21584819]
18. Wan XB, Long ZJ, Yan M, Xu J, Xia LP, Liu L, et al. Inhibition of Aurora-A suppresses epithelial-mesenchymal transition and invasion by downregulating MAPK in nasopharyngeal carcinoma cells. Carcinogenesis. 2008 Oct; 29(10):1930–1937. [PubMed: 18667445]
19. Tatsuka M, Sato S, Kitajima S, Suto S, Kawai H, Miyauchi M, et al. Overexpression of Aurora-A potentiates HRAS-mediated oncogenic transformation and is implicated in oral carcinogenesis. Oncogene. 2005 Feb 3; 24(6):1122–1127. [PubMed: 15592510]
20. Yang H, He L, Kruk P, Nicosia SV, Cheng JQ. Aurora-A induces cell survival and chemoresistance by activation of Akt through a p53-dependent manner in ovarian cancer cells. Int J Cancer. 2006 Nov 15; 119(10):2304–2312. [PubMed: 16894566]
21. Wu JC, Chen TY, Yu CT, Tsai SJ, Hsu JM, Tang MJ, et al. Identification of V23RalA-Ser194 as a critical mediator for Aurora-A-induced cellular motility and transformation by small pool expression screening. J Biol Chem. 2005 Mar 11; 280(10):9013–9022. [PubMed: 15637052]
22. Yeatman TJ. A renaissance for SRC. Nat Rev Cancer. 2004 Jun; 4(6):470–480. [PubMed: 15170449]
23. O'Neill GM, Seo S, Serebriiskii IG, Lessin SR, Golemis EA. A new central scaffold for metastasis: parsing HEF1/Cas-L/NEDD9. Cancer Res. 2007 Oct 1; 67(19):8975–8979. [PubMed: 17908996]
24. Pugacheva EN, Golemis EA. HEF1-aurora A interactions: points of dialog between the cell cycle and cell attachment signaling networks. Cell Cycle. 2006 Feb; 5(4):384–391. [PubMed: 16479169]
25. Ji H, Ramsey MR, Hayes DN, Fan C, McNamara K, Kozlowski P, et al. LKB1 modulates lung cancer differentiation and metastasis. Nature. 2007 Aug 16; 448(7155):807–810. [PubMed: 17676035]
26. Kim M, Gans JD, Nogueira C, Wang A, Paik JH, Feng B, et al. Comparative oncogenomics identifies NEDD9 as a melanoma metastasis gene. Cell. 2006 Jun 30; 125(7):1269–1281. [PubMed: 16814714]
27. Pugacheva EN, Golemis EA. The focal adhesion scaffolding protein HEF1 regulates activation of the Aurora-A and Nek2 kinases at the centrosome. Nat Cell Biol. 2005 Oct; 7(10):937–946. [PubMed: 16184168]
28. Mortlock A, Keen NJ, Jung FH, Heron NM, Foote KM, Wilkinson R, et al. Progress in the development of selective inhibitors of Aurora kinases. Curr Top Med Chem. 2005; 5(2):199–213. [PubMed: 15853647]
29. Manfredi MG, Ecsedy JA, Meetze KA, Balani SK, Burenkova O, Chen W, et al. Antitumor activity of MLN8054, an orally active small-molecule inhibitor of Aurora A kinase. Proc Natl Acad Sci U S A. 2007 Mar 6; 104(10):4106–4111. [PubMed: 17360485]
30. Manfredi MG, Ecsedy JA, Chakravarty A, Silverman L, Zhang M, Hoar KM, et al. Characterization of Alisertib (MLN8237), an investigational small-molecule inhibitor of aurora A kinase using novel in vivo pharmacodynamic assays. Clin Cancer Res. 2011 Dec 15; 17(24):7614–7624. [PubMed: 22016509]
31. Tikhmyanova N, Little JL, Golemis EA. CAS proteins in normal and pathological cell growth control. Cell Mol Life Sci. 2010 Apr; 67(7):1025–1048. [PubMed: 19937461]
32. Feki A, Berardi P, Bellingan G, Major A, Krause KH, Petignat P, et al. Dissemination of intraperitoneal ovarian cancer: Discussion of mechanisms and demonstration of lymphatic spreading in ovarian cancer model. Crit Rev Oncol Hematol. 2009 Oct; 72(1):1–9. [PubMed: 19179094]
33. Guarino M. Src signaling in cancer invasion. J Cell Physiol. 2010 Apr; 223(1):14–26. [PubMed: 20049846]

34. Anand S, Penrhyn-Lowe AR, Venkitaraman AR. Aurora-A amplificaiton overrides the mitotic spindle assembly checkpoint, inducing resistance to taxol. Cancer Cell. 2003; 3:51–62. 2003. [PubMed: 12559175]
35. Hata T, Furukawa T, Sunamura M, Egawa S, Motoi F, Ohmura N, et al. RNA interference targeting aurora kinase a suppresses tumor growth and enhances the taxane chemosensitivity in human pancreatic cancer cells. Cancer Res. 2005 Apr 1; 65(7):2899–2905. [PubMed: 15805292]
36. Mazumdar A, Henderson YC, El-Naggar AK, Sen S, Clayman GL. Aurora kinase A inhibition and paclitaxel as targeted combination therapy for head and neck squamous cell carcinoma. Head Neck. 2009 May; 31(5):625–634. [PubMed: 19107951]
37. Shimomura T, Hasako S, Nakatsuru Y, Mita T, Ichikawa K, Kodera T, et al. MK-5108, a highly selective Aurora-A kinase inhibitor, shows antitumor activity alone and in combination with docetaxel. Mol Cancer Ther. 2010 Jan; 9(1):157–166. [PubMed: 20053775]
38. Tanaka E, Hashimoto Y, Ito T, Kondo K, Higashiyama M, Tsunoda S, et al. The suppression of aurora-A/STK15/BTAK expression enhances chemosensitivity to docetaxel in human esophageal squamous cell carcinoma. Clin Cancer Res. 2007 Feb 15; 13(4):1331–1340. [PubMed: 17317845]
39. Wysong DR, Chakravarty A, Hoar K, Ecsedy JA. The inhibition of Aurora A abrogates the mitotic delay induced by microtubule perturbing agents. Cell Cycle. 2009 Mar 15; 8(6):876–888. [PubMed: 19221504]
40. Matsuo K, Eno ML, Im DD, Rosenshein NB. Chemotherapy time interval and development of platinum and taxane resistance in ovarian, fallopian, and peritoneal carcinomas. Arch Gynecol Obstet. 2010 Feb; 281(2):325–328. [PubMed: 19455347]
41. Chou TC. Theoretical basis, experimental design, and computerized simulation of synergism and antagonism in drug combination studies. Pharmacol Rev. 2006 Sep; 58(3):621–681. [PubMed: 16968952]
42. Luker KE, Luker GD. Applications of bioluminescence imaging to antiviral research and therapy: multiple luciferase enzymes and quantitation. Antiviral Res. 2008 Jun; 78(3):179–187. [PubMed: 18358543]
43. Lin YG, Immaneni A, Merritt WM, Mangala LS, Kim SW, Shahzad MM, et al. Targeting aurora kinase with MK-0457 inhibits ovarian cancer growth. Clin Cancer Res. 2008 Sep 1; 14(17):5437–5446. [PubMed: 18765535]
44. Harrington EA, Bebbington D, Moore J, Rasmussen RK, Ajose-Adeogun AO, Nakayama T, et al. VX-680, a potent and selective small-molecule inhibitor of the Aurora kinases, suppresses tumor growth in vivo. Nature. 2004; 10(3):262–267. 2004.
45. Payton M, Bush TL, Chung G, Ziegler B, Eden P, McElroy P, et al. Preclinical evaluation of AMG 900, a novel potent and highly selective pan-aurora kinase inhibitor with activity in taxane-resistant tumor cell lines. Cancer Res. 2010 Dec 1; 70(23):9846–9854. [PubMed: 20935223]
46. Komlodi-Pasztor E, Sackett DL, Fojo AT. Inhibitors targeting mitosis: tales of how great drugs against a promising target were brought down by a flawed rationale. Clin Cancer Res. 2012 Jan 1; 18(1):51–63. [PubMed: 22215906]
47. Huck JJ, Zhang M, McDonald A, Bowman D, Hoar KM, Stringer B, et al. MLN8054, an inhibitor of Aurora A kinase, induces senescence in human tumor cells both in vitro and in vivo. Mol Cancer Res. 2010 Mar; 8(3):373–384. [PubMed: 20197380]
48. Ratushny V, Pathak HB, Beeharry N, Tikhmyanova N, Xiao F, Li T, et al. Dual inhibition of SRC and Aurora kinases induces postmitotic attachment defects and cell death. Oncogene. 2012 Mar 8; 31(10):1217–1227. [PubMed: 21785464]
49. Tan DS, Agarwal R, Kaye SB. Mechanisms of transcoelomic metastasis in ovarian cancer. Lancet Oncol. 2006 Nov; 7(11):925–934. [PubMed: 17081918]
50. Swift, S.; Lorens, J.; Achacoso, P.; Nolan, GP. Current Protocols in Immunology. John Wiley & Sons, Inc.; 2001. Rapid Production of Retroviruses for Efficient Gene Delivery to Mammalian Cells Using 293T Cell–Based Systems.
51. Do TV, Symowicz JC, Berman DM, Liotta LA, Petricoin EF 3rd, Stack MS, et al. Lysophosphatidic acid down-regulates stress fibers and up-regulates pro-matrix metalloproteinase-2 activation in ovarian cancer cells. Mol Cancer Res. 2007 Feb; 5(2):121–131. [PubMed: 17314270]

52. Connolly DC, Hensley HH. Xenograft and Transgenic Mouse Models of Epithelial Ovarian Cancer and Non-Invasive Imaging Modalities to Monitor Ovarian Tumor Growth In Situ: Applications in Evaluating Novel Therapeutic Agents. Current Protoc Pharmacol. 2009; 45:14.2.1–14.2.36.

53. Connolly DC, Bao R, Nikitin AY, Stephens KC, Poole TW, Hua X, et al. Female mice chimeric for expression of the simian virus 40 TAg under control of the MISIIR promoter develop epithelial ovarian cancer. Cancer Res. 2003 Mar 15; 63(6):1389–1397. [PubMed: 12649204]

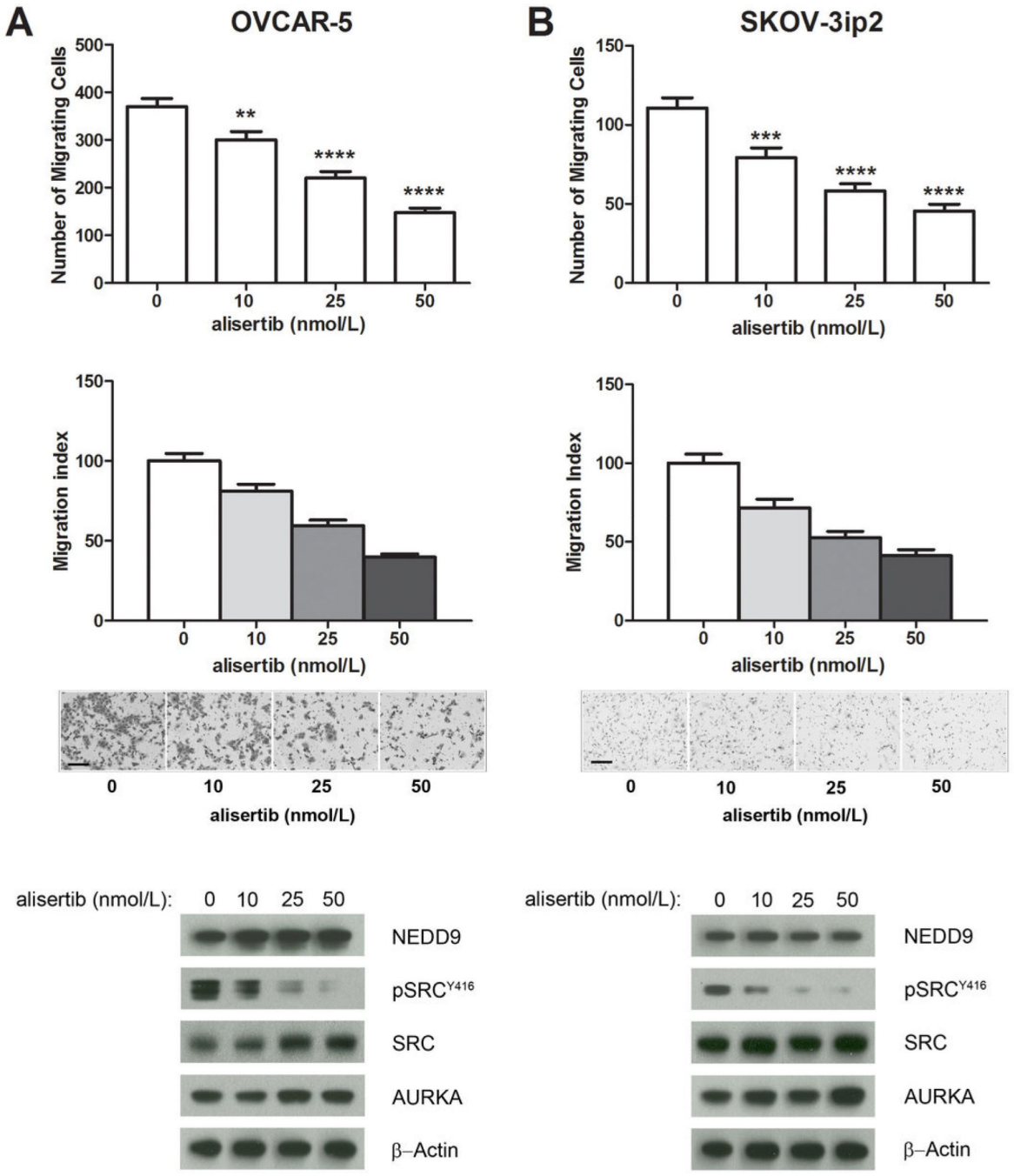

Figure 1. Treatment of ovarian carcinoma cells with the AURKA inhibitor alisertib inhibits migration

OVCAR-5 (A) and SKOV3ip2 (B) cells were treated with 0 (vehicle), 10, 25 and 50 nmol/L alisertib for 4 h, and then subjected to migration assays. Quantification of migration for OVCAR-5 (A) and SKOV3ip2 (B) is depicted as the mean number of migrating cells ± SE ($n = 3$). Bars labeled with asterisks are statistically significant (**$P < 0.01$, ***$P < 0.001$ and ****$P < 0.0001$) as analyzed by one-way ANOVA Kruskal-Wallace test followed by Dunn's multiple comparison test and Mann-Whitney tests comparing individual columns. The migration index (relative to vehicle-treated control) is depicted as the mean relative to vehicle-treated cells ± SE. Bright-field images (10×) of migrating cells from representative

inserts are shown (scale bar = 100 μm). Total proteins from cells treated for 24 h with 0, 10, 25 and 50 nmol/L alisertib were immunoblotted with antibodies against NEDD9, $pSRC^{Y416}$, total SRC, AURKA and β-Actin (loading control).

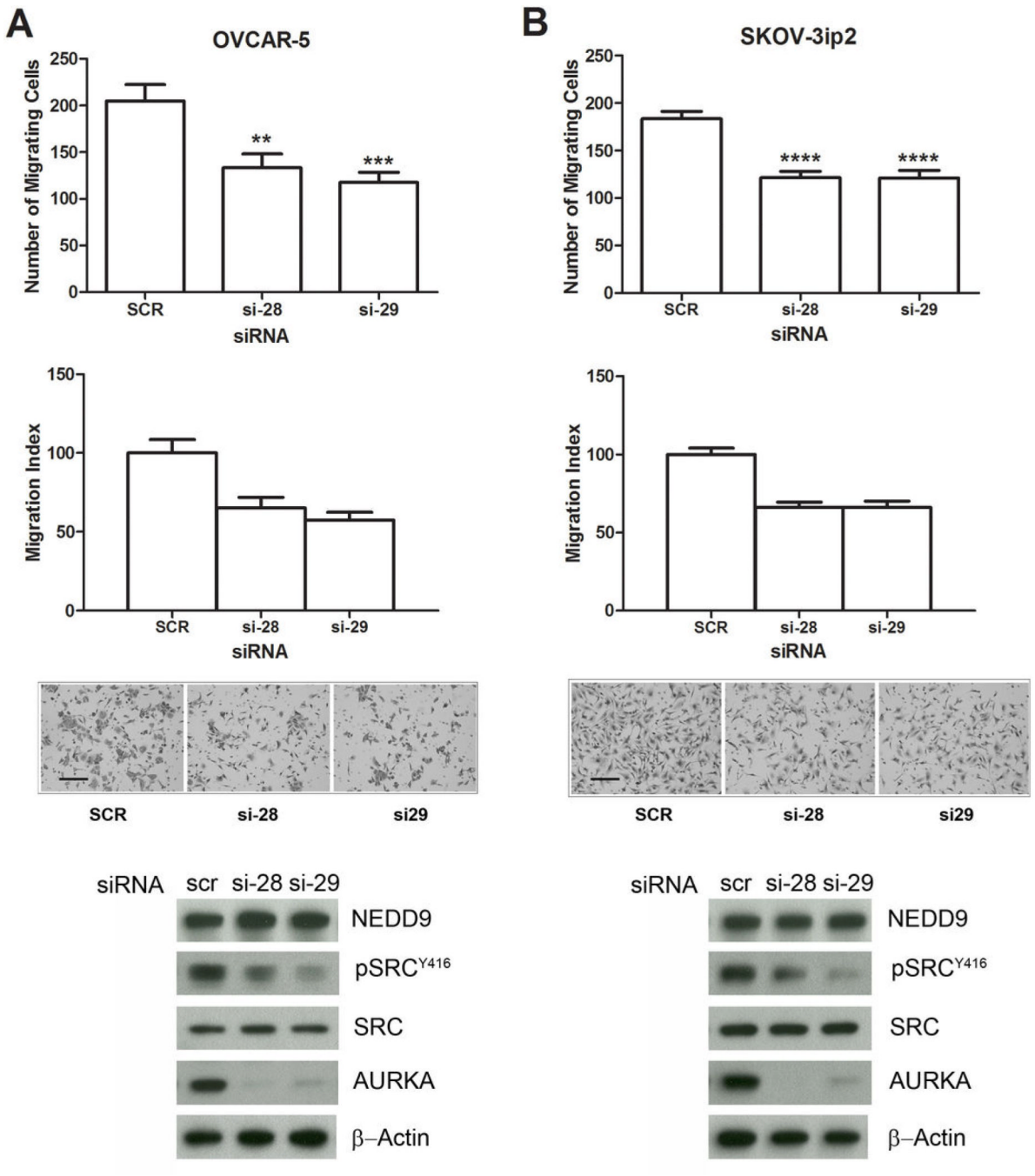

Figure 2. RNAi-mediated silencing of *AURKA* inhibits ovarian carcinoma cell migration

OVCAR-5 (A) and SKOV3ip2 (B) cells were transiently transfected with non-targeting scrambled (SCR) *AURKA*-specific siRNAs (si-28 and si-29) for 48 h, and then subjected to migration assays or immunoblot analysis. Quantification of migration for OVCAR-5 (A) and SKOV3ip2 (B) is depicted in the top graphs as the mean number of migrating cells ± SE ($n = 3$). Bars labeled with asterisks are statistically significant (**$P < 0.01$, ***$P < 0.001$ and ****$P < 0.0001$) as analyzed by one-way ANOVA Kruskal-Wallace test followed by Dunn's multiple comparison test and Mann-Whitney tests comparing individual columns. The migration index is depicted in the bottom graphs as the means relative to SCR siRNA-

transfected cells ± SE. Bright-field images (10×) of migrating cells from representative inserts are shown (scale bar = 100 μm). Total protein lysates from cells transfected with SCR or *AURKA*-siRNAs (si28 and si-29) were immunoblotted with antibodies against NEDD9, $pSRC^{Y416}$, total SRC, AURKA, and β-Actin (loading control).

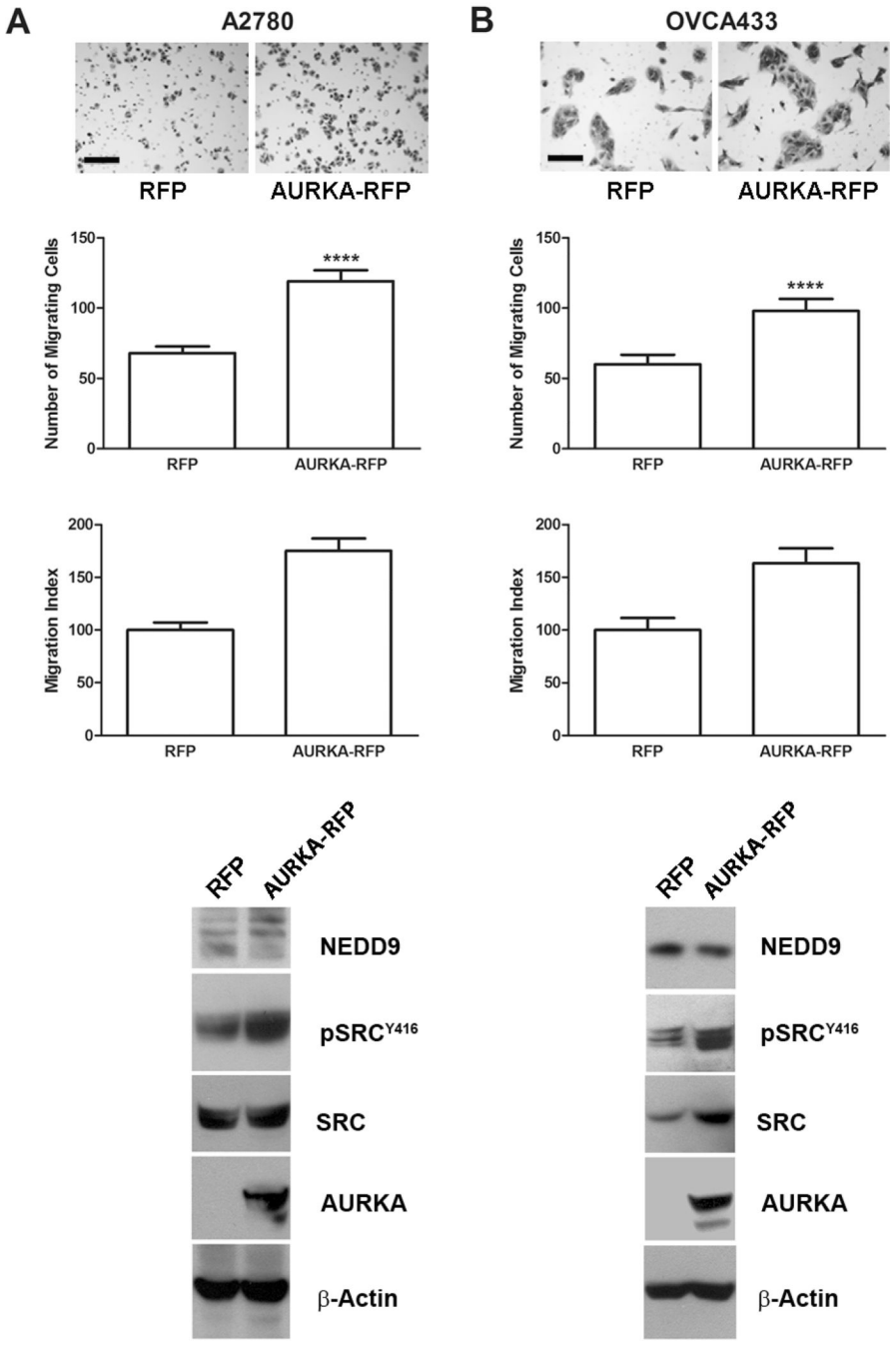

Figure 3. Enforced expression of *AURKA* stimulates ovarian carcinoma cell migration

A2780 (A) and OVCA433 (B) cells were transiently transfected with an *RFP* expression construct or an *AURKA-RFP* expression construct for 24 h and then subjected to migration assays and immunoblot analyses. Bright-field images (10×) of migrating cells from representative inserts are shown (scale bar = 100 μm). Quantification of migration for A2780 (A) and OVCA433 (B) is depicted in the top graphs as the mean number of migrating cells ± SE ($n = 3$). Bars labeled with asterisks are statistically significant (****$P < 0.0001$) as analyzed by the Mann-Whitney test. The migration index (relative to vehicle-treated control) is depicted in the bottom graphs as the mean relative to *RFP*-transfected

cells ± SE. Total proteins from cells transfected with *RFP* and *AURKA-RFP* were also immunoblotted with antibodies against NEDD9, $pSRC^{Y416}$, total SRC, AURKA, and β-actin (loading control).

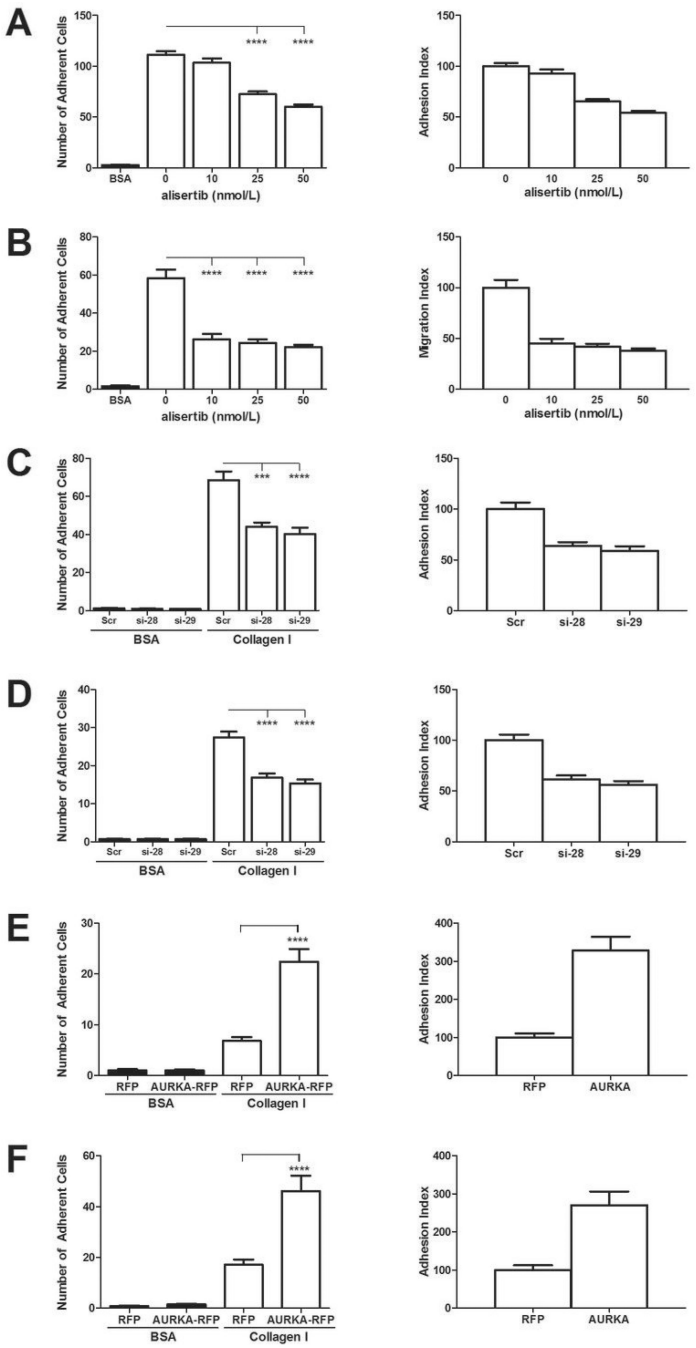

Figure 4. AURKA regulates ovarian carcinoma cell adhesion

The effects of altering AURKA expression/activity on cell adhesion were assayed by plating cells on 96-well plates coated with type I collagen or BSA (negative control). Adhesion was quantified by counting five different fields of cells in quadruplicate wells. Treatment of OVCAR-5 (A) and SKOV3ip2 (B) cells for 6 hr with increasing concentrations of alisertib (10, 25, 50 nmol/L) decreased cell adhesion to type I collagen compare to vehicle (DMSO) treated control cells. Silencing of *AURKA* by transient transfection of OVCAR-5 (C) and SKOV3ip2 (D) cells with *AURKA*-specific siRNAs (si-28 and si-29) decreased cell adhesion to type I collagen compared to cells transfected with scrambled (Scr) siRNA.

Overexpression of AURKA by transient expression of *AURKA-RFP* in A2780 (E) and OVCA433 (F) cells resulted in increased adhesion compared to *RFP* vector control transfected cells. For all cell lines, quantification of cell adhesion is depicted in the graphs on the left as the mean number of adherent cells ± SE ($n = 3$ independent experiments). The adhesion index (relative to control) is depicted in the graphs on the right as the mean relative to control cells ± SE ($n = 3$). Bars labeled with asterisks are statistically significant as analyzed by one-way ANOVA Kruskal-Wallace test followed by Dunn's multiple comparison test and Mann-Whitney tests comparing individual columns (***$P < 0.001$ and ****$P < 0.0001$).

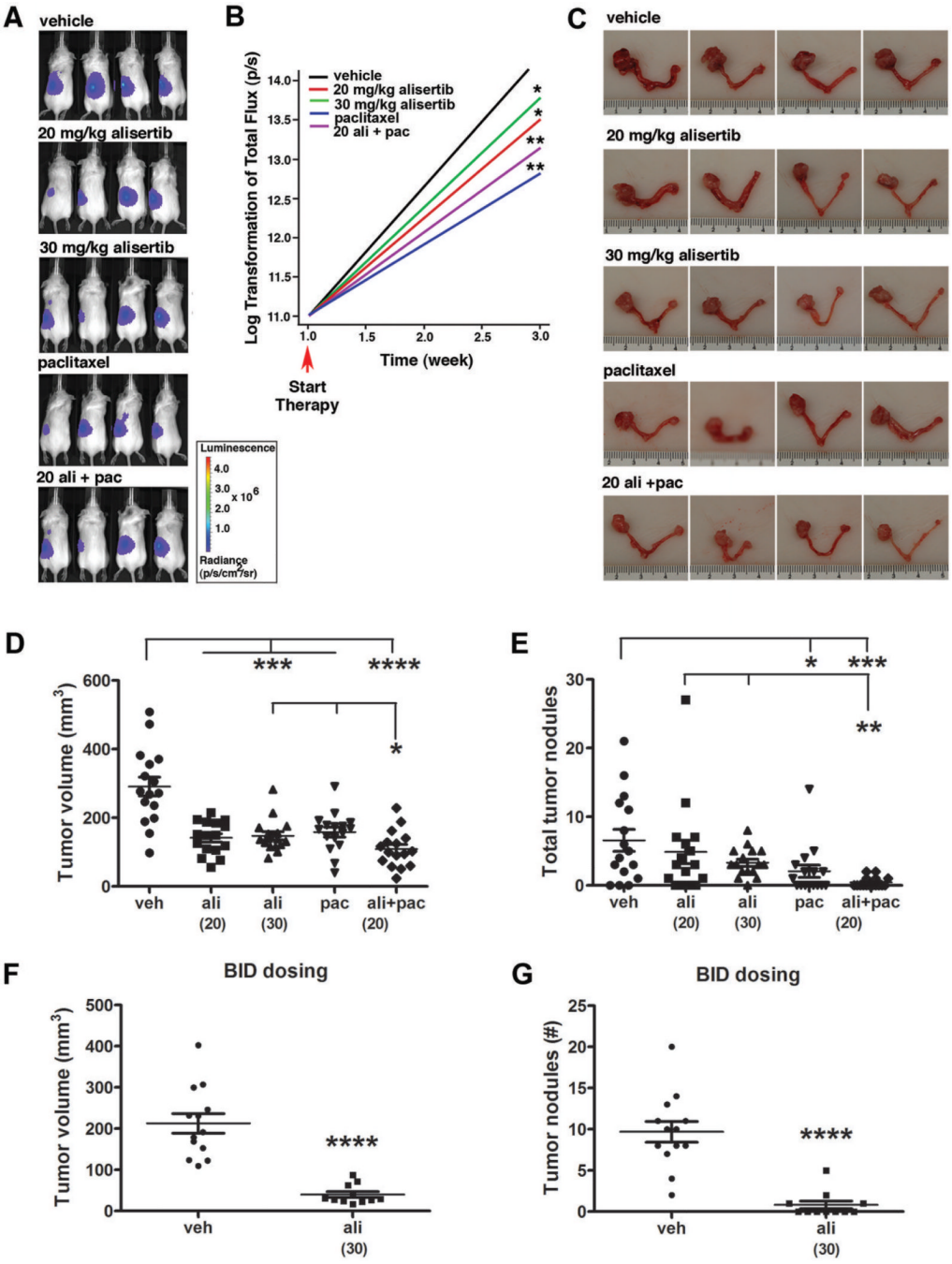

Figure 5. Alisertib alone or in combination with paclitaxel inhibits ovarian carcinoma growth and dissemination

(A) Representative bioluminescent images of mice treated for two weeks with: vehicle (veh), 20 mg/kg alisertib (ali), 30 mg/kg alisertib, 5 mg/kg paclitaxel (pac), and 20 mg/kg alisertib + paclitaxel (20 ali + pac). (B) Average tumor growth rate as determined from weekly BLI scans for each treatment group. One-sided Wilcoxon test showed the differences in growth rates were statistically significant from vehicle control (*, $P < 0.05$ and ***, $P < 0.001$). (C) Gross images of reproductive tracts from representative mice from each treatment group. (D) Vertical scatter plot depicting tumor volumes calculated from caliper measurements of the primary ovarian tumor for mice in each treatment group where groups

labeled with asterisks are statistically significant from vehicle control or from mice treated with combination of ali+pac compared to mice treated with ali or pac alone (*$P < 0.05$, ***$P < 0.001$ and ****$P < 0.0001$) as analyzed by the Mann-Whitney test. (E) Vertical scatter plot depicting the total number of tumor nodules present in the abdominal cavity for mice from each treatment groups is shown. Groups labeled with asterisks are statistically significant from vehicle control labeled with asterisks are statistically significant from vehicle control or from mice treated with combination of ali+pac compared to mice treated with ali or pac alone (*$P < 0.05$, **$P < 0.01$ and ***$P < 0.001$). In a separate experiment, mice treated twice daily with 30 mg/kg alisertib (n=11 mice) exhibited significantly decreased tumor volume (F) and total number of tumor nodules in the abdominal cavity (G) compared to vehicle (n=13 mice) treated controls (****$P < 0.0001$).

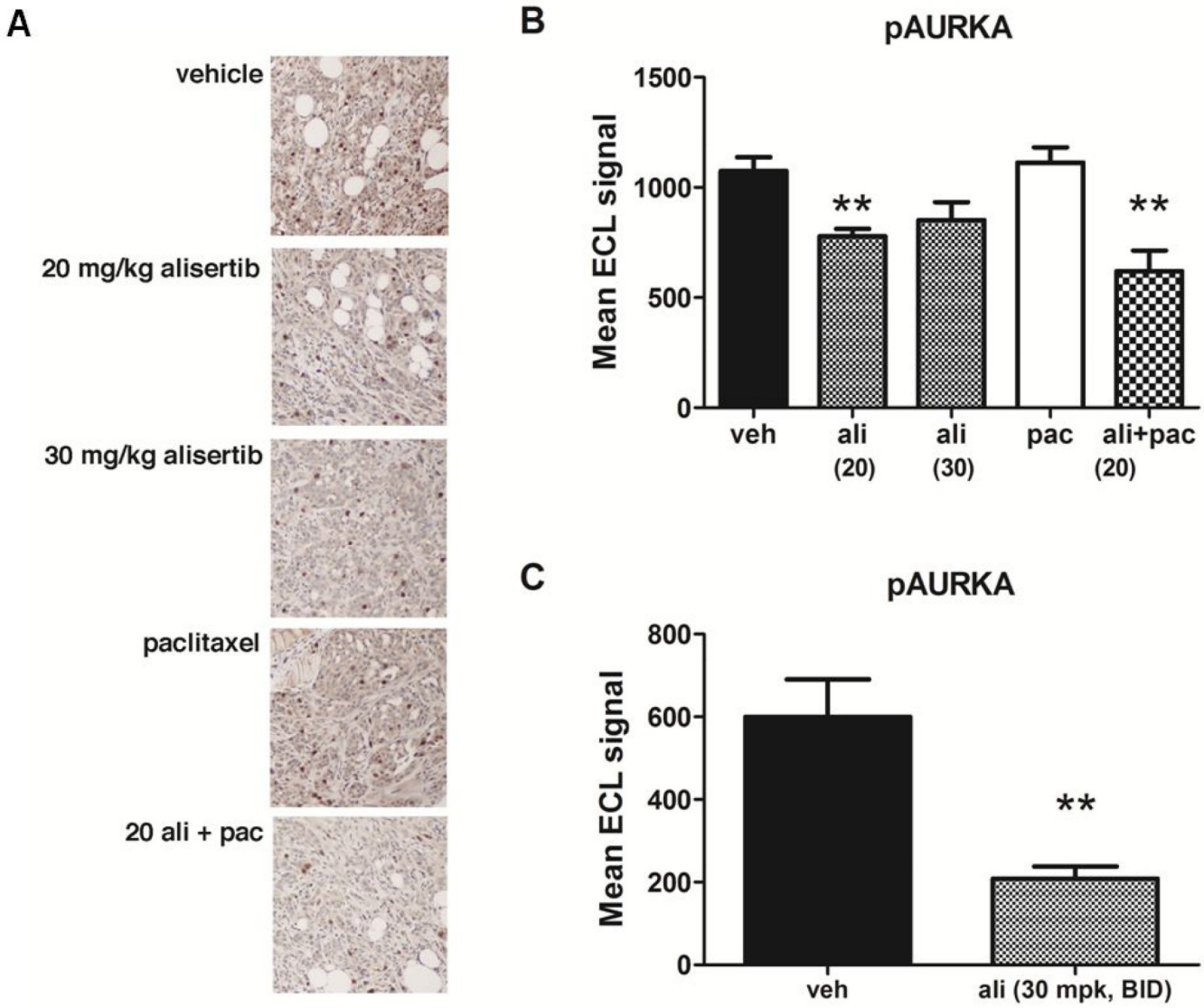

Figure 6. Alisertib treatment inhibits AURKA activation in tumors

Tumor samples from control and drug-treated mice were subjected to immunohistochemical or electrochemiluminescent ELISA detection of pAURKA^{T288}. A) Immunohistochemical detection of pAURKA^{T288} in tumor sections. The same exposure time was used to capture all images and the scale bar = 50 μm. B and C) ELISA detection of pAURKA^{T288} in total tumor protein lysates showed significantly lower levels of AURKA activation in mice treated with alisertib alone or in combination with paclitaxel compared to vehicle-treated controls (**$P < 0.01$).